Journal of Experimental and Clinical Medicine
https://dergipark.org.tr/omujecm

Research Article

J Exp Clin Med
2023; 40(4): 755-767
doi: 10.52142/omujecm.40.4.17

Roscovitine inhibits glycogen synthase kinase 3 beta signaling and exerts apoptotic effect with an increase in reactive oxygen species generation in neuroblastoma cells

Zeynep DEMİREL[1], Esranur KOPAL[1], Nilay DİNÇKURT[1], Berkay GÜRKAN[2] Ayşe KESKİN GÜNAY[3], Elif Damla ARISAN [4], Pınar OBAKAN YERLİKAYA[1,3,*]

[1]Department of Molecular Biology and Genetics, Istanbul Medeniyet University, İstanbul, Türkiye
[2] Department of Molecular Biology and Genetics, Istanbul Kültür University, İstanbul, Türkiye
[3]Science and Advanced Technologies Research Center, Istanbul Medeniyet University, İstanbul, Türkiye
[4]Biotechnology Institute, Gebze Technical University, Kocaeli, Türkiye

Received: 26.07.2023 • **Accepted/Published Online:** 10.10.2023 • **Final Version:** 29.10.2023

Abstract

Roscovitine (ROSC) is a selective cyclin-dependent kinase (CDK) inhibitor against CDK2, 7 and 9. ROSC's anti-proliferative and anti-cancer activities have been well-documented in both *in vivo* and *in vitro* studies against several cancer types. Glycogen synthase kinase 3 (GSK3) is a serine/threonine protein kinase that has a role in the regulation of glycogen synthase. It also has a role in multiple cellular processes and disease conditions. A member of the GSK3 family, GSK3β, has been implicated in many human malignancies including neuroblastoma. The specific inhibition of GSK3β reduced neuroendocrine markers and suppressed neuroblastoma (NB) cell growth. NB is a malign pediatric disease with diverse types of tumors and high heterogeneity. Lately, GSK3β targeted therapy models are being investigated for NB therapy. The action of ROSC on GSK3β, however, is not fully understood. In this study, we showed that ROSC exerts anti-proliferative and apoptotic activity in SK-N-AS neuroblastoma cells by increasing reactive oxygen species (ROS) generation, which can be prevented by N-acetyl-cysteine administration. ROSC treatment inhibited GSK3β signaling by promoting Ser9 inhibitory phosphorylation. ROSC at low doses can be a drug candidate to modulate GSK3β signaling in NB cells.

Keywords: Neuroblastoma, roscovitine, cell cycle, Apoptosis, GSK3β

1. Introduction

As an extracranial solid tumor, NB is the second most frequent cancer in children, indicated as the neural crest-derived malignancy of the peripheral nervous system. NB might manifest anywhere along the sympathetic nervous system; however, most tumors are in the adrenal gland medulla and the abdomen (1–3). NB attributes disproportionately, significant morbidity and mortality can be seen among children, or sometimes they can develop into a benign ganglioneuroma, and even a spontaneous and complete regression can be detected (4,5). Therefore, NB is remarkable because of its heterogeneity. Disseminated metastases are present in nearly 75% of cases in children over the age of 1. Stage IV usually represents an aggressive tumor resistant to chemotherapy and is generally untreatable. The molecular mechanisms lying behind the NB are usually somatic genetic alterations, which lead to overexpression of oncogenes and inactivation of tumor suppressor genes. For instance, 20% to 25% of NB cases occur due to the amplification of MYCN proto-oncogene (6). Lately, anaplastic lymphoma kinase (ALK) was also identified as an oncogene related to NB diagnosis (7). Besides, deletions in chromosomes 1p and 11q have also been detected and constitute a poor prognosis in patients (8,9). Recently, altered GSK3 (glycogen synthase kinase) expression was observed in NB patients due to its role in MYCN regulation (10). Studies indicated that GSK inhibitors can induce cell death in cancer cells via apoptosis (11–13). Duffy et al. showed that GSK3 inhibitor-treated NB cells exhibited altered multiple signaling pathways that contributed to the loss of cell viability (10). In addition, a GSK3 inhibitor, lithium chloride, successfully induced cancer cell death without causing harmful effects to epithelial cells (14,15).

Glycogen synthase kinase 3β (GSK3β) is a critical serine/threonine kinase in glycogen metabolism (16). There are two isoforms in mammals, GSK3α and β, weighing 51 and 47 kDa, respectively. In addition, GSK3β is also highly expressed in the central nervous system and stabilizes microtubule-associated proteins via phosphorylation (17). For this reason, GSK3β deprivation causes fatal consequences in the embryonic stage. GSK3β activity is tightly regulated in cells, especially from the Serin 9 and Serin 21 residues at the N-

*Correspondence: pinar.obakan@medeniyet.edu.tr

terminus of the protein. Upon the inhibitory phosphorylation from these residues, the release of axin and β-catenin from the complex occurs, leading to the translocation of β-catenin to the nucleus. β-catenin, a transcription factor, migrates to the nucleus and coordinates the expression of essential factors in neuron survival, such as c-Jun (18). In addition, the Wnt signaling pathway inhibits GSK3β activity by causing phosphorylation of the Serine (Ser) 9 residue (19). With this regulation, GSK3β is involved in many cell signaling pathways, such as cell adhesion, division, transcription mechanism, and tau phosphorylation. Therefore, GSK3β is associated with many pathological conditions as a molecular target. In addition to the phosphorylation of β-catenin in the sub-signaling pathways, it plays a decisive role in cell survival-death fate with its effects on c-Jun and interacting with IRS-1 (20). GSK3β is an essential factor for neuronal cell survival. However, excessive GSK3β activity can cause cell death for many cell types and neurons (21).

Among the 538 human kinases, cyclin-dependent kinases (CDKs) were examined in detail since they have significant roles in cellular processes such as cell division and cell death (22,23). The cell cycle process is a remarkably conserved phenomenon in eukaryotes, and it is highly regulated to provide proper cell division. As said before, CDKs have critical functions as cell cycle regulators working with other associated cyclins to arrange the cell cycle progression. CDK1, CDK2, CDK4, and CDK6 are essential for DNA replication, mitotic progression, and growth regulatory signal responses; however, transcriptional regulation of CDK7, CDK8, and CDK9 also plays a role (24). Abnormal activation of CDKs leads to abnormal cell cycle progression and tumorigenesis. Therefore, pharmacological inhibitors of CDKs are attracting attention as potential anti-cancer agents, encouraging scientists to optimize and characterize, revealing a new strategy for cancer therapy (23).

Roscovitine (ROSC) is a CDK inhibitor, a purine derivative that inhibits CDK1, CDK2, CDK5, CDK7, and CDK9. However, it is an inhibitor with weak binding to CDK4, CDK6, and CDK8 (25). It shows an affinity for the ATP binding cleft of the kinase in competition with ATP. This binding in the catalytic region occurs by direct co-crystallization with CDK2 (26). It is a synthetic inhibitor studied in clinical studies as a candidate drug for some oncogenic indications (27). ROSC's anti-tumor activity in various cancer types was demonstrated on multiple cell lines (28). The therapeutic efficacy of ROSC against neurodegenerative diseases, cardiovascular disorders, viral infections, and parasitic protozoa was investigated at the preclinical level (29). In addition, ROSC is used for macrophage function and killing multi-drug-resistant bacteria (30). Although there is a wide variety of protein kinase inhibitors, the search for their optimization and characterization continues and offers promising results. In addition, ROSC exerts a synergistic effect with anti-cancer agents such as doxorubicin, taxol, 5-fluorouracil, vinblastine, alemtuzumab, paclitaxel, trastuzumab, cisplatin, radiation, irinotecan, etoposide, and tamoxifen (31). Phase I and II trials of ROSC were carried out in various cancer treatments and tested in monotherapy and combination therapies (32). ROSC treatment induced cell cycle arrest and apoptosis in many cancer types. This process affects many pathways, including RAS-MAPK, NF-κB, p53, estrogen receptor, and JAK-STAT signaling pathways (31). In addition to in vitro experiments, *in vivo* analyses were carried out, and the effects of ROSC in mono and combined therapies were investigated in various mouse and rat models (33). Studies have shown that Tau protein has serine and threonine phosphorylation sites targeted by protein kinases such as GSK3β and CDK5 (34). ROSC, a CDK inhibitor, is also seen as a potential GSK3β inhibitor. Inhibition of CDK5 by ROSC has neuroprotective effects in the modulation of Tau / GSK3β and ERK / PPARγ / CREB signals in neuronal damage and cognitive dysfunction (35). In addition, the ROSC effect in GSK3β signaling was detected in Human T-cell leukemia virus type I (HTLV-I) cells (36). It is also known that the therapeutic agent ROSC shows GSK3β activity in combined applications in the treatment process of Alzheimer's disease (AD) (37). In light of the above literature data, this study aims to understand the anti-cancer properties of ROSC as a CDK and potential GSK3β inhibitor.

2. Materials and methods

2.1. Cell Culture

The NB cell line SK-N-AS (CRL-2137) was obtained from the American Type Culture Collection (ATCC). Cells were grown in DMEM (Dulbecco's Modified Eagle Medium) medium containing 10% fetal bovine serum, 10 U/ml penicillin/streptomycin antibiotic supplement, and 0.1 mM non-essential amino acid and incubated 5% CO2 incubator at 37 °C (Heracell 150; Thermo Electron Corporation, Waltham, MA, USA).

2.2. MTT Assay

Cells were seeded at 1 x 10^4 density per well in 96-well plates and exposed to 1 and 10 μM ROSC for 24 h. 10 μl 3-(4,5-dimethylthiazol-2-yl)-2,5- diphenyl tetrazolium bromide dye (5 mg/ml) (Roche, Indianapolis, USA) was added to each well and cells were kept at 37ºC for 4 h. The resulting formazan crystals were solubilized in 200 μl dimethyl sulfoxide (DMSO). The density of the solubilized formazan was read at 570 nm spectrophotometrically (Bio-Rad, Hercules, CA, USA) (38).

2.3. Trypan Blue Dye Exclusion Assay

Cells were seeded at 1 × 10^5 density in 6-well plates (TPP, Zollstrasse, Switzerland) and treated with ROSC dose-dependently within 96h. After trypsinization (Trypsin EDTA (0.25%), Gibco, USA), and centrifugation, cells were exposed to 0.4% (w/v) Trypan Blue (Gibco -Life Technologies, USA) and cell culture media at a 1:1 ratio. 10 μL of cells were counted by a dual-chamber 0.1 mm deep Neubauer improved hemocytometer (39).

2.4. Clonogenic Assay

Cells were seeded at 1 × 10^4 density into 6-well plates and treated with increasing concentrations of ROSC for 24 h. Then, the media was removed, and cells were washed with 1X PBS fixed with methanol:acetic acid (3:1) for 5 min. Following the removal of the fixing agent, cells were stained with 0.5% crystal violet in methanol for 30 min, washed with distilled water, and the images were taken under light microscopy (40).

2.5. Soft agar colony formation assay

A mixture containing a 1:1 ratio of DMEM (20% FBS and 2% penicillin/streptomycin) and 1% agar was prepared for soft agar analysis. The resulting mixture was distributed as 1 ml per well on 6-well plates and incubated until solidification. Later, 2.5×10^5 cells (untreated or treated samples) were added to each well with 0.5 % agar and were applied at a 1:1 ratio with 2X DMEM medium. Samples were incubated at 37 °C for 15 days and visualized under the light microscope (Olympus, IX70) (41).

2.6. Fluorescence Microscopy

2.6.1. *Propidium iodide staining*

SK-N-AS cells ($1x10^5$) were seeded into 12 well plates and treated with ROSC (0-30 µM) for 24 h. Following a dose-dependent ROSC treatment, the cells were washed once with 1X PBS and stained with propidium iodide (PI) (50 mg/ml stock concentration in 1X PBS) fluorescent probe and were incubated for 10 min in the dark. ROSC-induced cell death was detected with fluorescence microscopy (Olympus, Tokyo, Japan) (42).

2.6.2. *3,3'-Dihexyloxacarbocyanine iodide (DiOC6) staining*

SK-N-AS cells were seeded at a density of $1x10^5$/ well into 12 well plates. Following exposure of cells to ROSC (0-30µM), they were washed once with 1X PBS and then stained with 4 nM 3,3'-dihexyloxacarbocyanine iodide (DiOC6) (40 nM stock concentration in DMSO; Calbiochem, La Jolla, CA, USA) fluorescent probe. Mitochondrial membrane potential (MMP) disruption was visualized by fluorescence microscopy (Zeiss, AX10) (excitation/emission: 482/ 504 nm) (43).

2.6.3. *4',6-diamidino-2-phenylindole (DAPI) staining*

The cells were seeded in 12-well plates at 1x105 cells/well density and treated with purvalanol (0-30 µM) for 24 h. After treatment, the cells were washed once with 1X PBS. The cells were stained with 1 µl/ml 4',6-diamidino-2-phenylindole (DAPI) (1 mg/ml stock concentration in 1X PBS) fluorescent probe and were incubated for 10 min in the dark. Dose-dependent ROSC-induced nuclear DNA fragmentation was visualized using fluorescence microscopy (Zeiss, AX10) (excitation/emission: 350/ 465 nm) (44).

2.6.4.*2',7'-dichlorofluorescein-diacetate(DCFH-DA) staining*

Fluorometric analysis of DCFH-DA staining

After drug administration in cell culture, cells were stained with DCFH-DA (1 µM final concentration) and incubated at 37 °C for 10 min. Cells were washed with 1X PBS and analyzed with the Accuri C6 flow cytometer (BD Biosciences, Oxford, UK). Data analysis was performed with the BD Accuri C6 software (BD Biosciences) (excitation/emission: 495/529 nm) (45).

2.7. Protein isolation and immunoblotting

SK-N-AS cells were seeded in 60 mm^2 Petri dishes at a $5x10^5$ density. Following the seeding overnight, they were exposed to increasing concentrations of ROSC for 24h. Later, cells were collected twice by scraping using 1X PBS and precipitated by centrifugation at 13,200 rpm for 1 min. After removing the supernatant, M-PER lysis buffer was added to the cells (Thermo Fischer Scientific). The samples were incubated for 20 min. at RT in a shaker and later were centrifuged at 13,200 rpm for 20 min at +4 °C. The supernatants were kept as total protein isolates at -80°C. PhosSTOP (Sigma Aldrich, Schnelldorf, Germany) was used during phosphorylated protein isolation. NE-PER Nuclear and Cytoplasmic Extraction protocol (Thermo Fisher Scientific) was followed for the nuclear and cytoplasmic protein isolation. The Bradford method was used for protein quantification, and bovine serum albumin (BSA) was used for the standard curve graphs. For the immunoblotting, isolated proteins were mixed with 4X Laemmlli loading buffer, kept for 5 min at 95 °C, and 30 µg protein samples were loaded into 12% acrylamide/bis-acrylamide gels. Following the running step, samples were transferred to polyvinyl fluoride (PVDF) membranes activated by methanol. Later, membranes were blocked using 5% skim milk prepared in 1X TBS containing 0.1% Tween 20 (TBS-T) at RT for 1h. After the blocking step, membranes were incubated at +4 °C with the selected primary antibodies at a ratio of 1:1000 (Cell Signaling Technology). Following washing steps with 1X TBS-T, membranes were incubated with secondary antibodies overnight. The secondary antibody application was followed by the washing step and subjected to a chemiluminescence solution. The signals from HRP-conjugated secondary antibodies were detected by the Chemidoc MP Imaging system (Bio-Rad Laboratories, Hercules, CA). All results were repeated at least three times, and the representative blots were given (39).

2.8. Flow cytometric analysis of apoptosis

$2x10^5$ cells/well were seeded in 6 well plates and treated with increased concentrations of ROSC for 24 h. Later, cells were collected following trypsinization and the cell pellet were collected and re-suspended in 300 µl of binding buffer with RNase (100 µg/ml), 3 µl FITC-conjugated annexin V, and 3 µl propidium iodide (PI, BD Biosciences, San Jose, CA, USA) obtained with FITC Annexin V Apoptosis Detection Kit I (BD Biosciences, Bedford, MA).

Samples were kept for 15 min at 37 °C in the dark. Later, the obtained samples were analyzed by BD Accuri C6 software (BD Biosciences) (46).

2.9. Cell cycle analysis

Cells were seeded in six-well plates with a density of $5x10^5$ cells/well; following 24 h 1 and 10 μM of ROSC treatment, drug-containing media were discarded, and the cells were collected by trypsinization. Following a centrifuge step at 13,200 orm for 2 min, the pellet was kept, and cells in the pellet were fixed in 70% ethanol. Cell suspensions were exposed to RNaseA and propidium iodide for staining. The cell cycle distribution was then analyzed by flow cytometry using BD Accuri C6 software (BD Bioscience) (46).

2.10. Statistics

All the experiments were statistically analyzed by GraphPad Prism 9 software (http://www.graphpad.com/). Error bars in the graphs were generated using ± standard deviation (SD) values. A statistical significance test was utilized by using ANOVA Bonferroni's multiple comparisons test. *$p<0.05$ was taken as a level of significance. Results were repeated at least three times. The immunoblotting results shown are representative of three separate experiments.

3. Results

3.1. Roscovitine treatment decreased cell viability and survival of SK-N-AS cells

To check the effects of ROSC on the cell viability of the SK-N-AS cells, an MTT assay was performed. ROSC was delivered to cells with increasing doses (0-50 μM). The results from three separate experiments were analyzed and shown in Fig. 1A. 1 and 10 μM ROSC treatment caused a significant reduction in viability, especially in 10 μM concentration. The trypan blue dye exclusion results are shown in a time-dependent manner in Fig. 1B. SK-N-AS cells were treated with 1 and 10 μM ROSC in a time-dependent manner for 96h, and the cells were counted with a hemocytometer. The numbers of viable cells were given in a graph. The number of cells treated with 10 μM ROSC was significantly reduced compared to control untreated cells or treated with 1 μM ROSC. Later, we investigated the apoptotic potential of ROSC on SK-N-AS cells. Following the exposure of cells to 1 and 10 μM ROSC for 24 h, bright DAPI-stained nuclei were observed dose-dependently under a fluorescent microscope, suggesting the DNA condensation might increase because of the drug treatments. We also observed that the PI stained cells significantly increased, especially after 10 μM ROSC treatment, indicating that dead cells accumulate following 24h at higher concentrations (Fig. 1C). Finally, diminished fluorescence was observed in cells with disrupted mitochondrial membrane potential loss, which was detected with $DiOC_6$ staining following cell exposure to increasing ROSC concentrations in SK-N-AS cells.

3.2. ROSC treatment decreased the colony formation potential of SK-N-AS cells

We also investigated the ability of ROSC to diminish the colony formation potential of SK-N-AS NB cells. To better visualize the ROSC effect, we seeded an increasing number of cells, $5x10^3$ and $7.5x10^{2,}$ respectively, in a 6-well plate and exposed to 1 and 10 μM ROSC for 24h. Fig. 2A showed a remarkable difference in the colonies formed, especially after 10 μM ROSC doses. The effect of ROSC on colony formation was also determined with a soft agar assay. The diameters of the colonies were significantly reduced or completely disappeared after 10 μM ROSC treatment. A similar effect was not observed after the exposure of cells to 1 μM ROSC.

3.3. ROSC triggered apoptotic cell death in SK-N-AS cells

Flow cytometric analyses were performed to demonstrate the efficacy of ROSC in triggering apoptosis and to evaluate the cell cycle distribution following 1 and 10 μM ROSC treatment in SK-N-AS cells. When the quadrants were analyzed, it was clear that as the doses of the administered drug increased, the early and late apoptotic population percentages elevated (Fig. 3A). In addition, we also determined that 1 μM ROSC treatment caused a subG1 population percentage increase. However, the number of viable cells was low rather than a dose-dependent increment in subG1 population percentage, and the cycle distribution after 10 μM ROSC exposure did not change (Fig. 3B). Since the annexinV-PI staining and the increase in subG1 populations were observed in SK-N-AS cells due to ROSC treatment, we investigated the expression of pro- and anti-apoptotic proteins by immunoblotting. For this purpose, we evaluated Puma, Bid, Bax, and pro-caspase 9, caspase 3 and 7, Bcl-2, Bcl-x_L, and PARP expressions. We observed no significant expression change in Puma after 1 mM ROSC treatment; however, a 10 μM dose was able to diminish it. The sharp decrease in Bid levels as a response to ROSC treatment indicated that the extrinsic apoptosis pathway might also be affected (Fig. 3C). While Bax protein levels elevated after 1 μM of the drug, the expression level was controlled after 10 μM drug exposure to SK-N-AS cells (Fig. 3C).

On the other hand, anti-apoptotic Bcl-2 and Bcl-x_L protein expressions were downregulated time-dependently, which demonstrates that mitochondria-dependent apoptosis was induced after ROSC treatments (Fig. 3C). When we checked the expression profiles of caspase proteins, we observed that pro-caspase9 significantly decreased after drug exposure dose-dependently, and the active forms of caspase 3 and 7 were elevated. As a direct proof of apoptosis, the cleavage of PARP protein was observed following 10 μM ROSC treatment in SK-N-AS cells.

3.4. Reactive oxygen species played a role in ROSC-induced apoptosis in SK-N-AS cells

To understand whether ROS levels were affected by ROSC treatment in SK-N-AS cells and whether the elevated levels of ROSC are related to cell viability loss, we performed fluorescence staining and flow cytometry using DCFH-DA. First, flow cytometry determined a significant increase in ROS levels in both 1 and 10 μM ROSC-treated cells (Fig. 4A). The increase was calculated as 2-fold and 2.5-fold for 1 and 10 μM ROSC treatments compared to control samples in SK-N-AS cells (Fig. 4A). Later, we used NAC as a ROS scavenger to ensure that ROS levels affect cell viability after ROSC

treatments. First, we determined whether DCFH-DA levels changed after NAC combined treatment with ROSC. As shown in Fig. 4B, NAC presence diminished the ROSC-induced ROS production by 3-fold (Fig. 4B). NAC itself did not cause ROS production. Later, we also observed that decreased relative cell viability, approximately 50% by 10 µM ROSC treatment, was completely restored with the combined treatment of NAC and 10 µM ROSC (Fig. 4C).

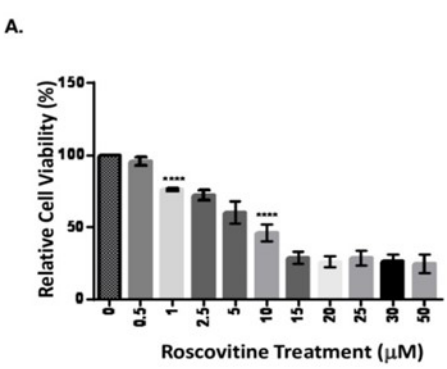

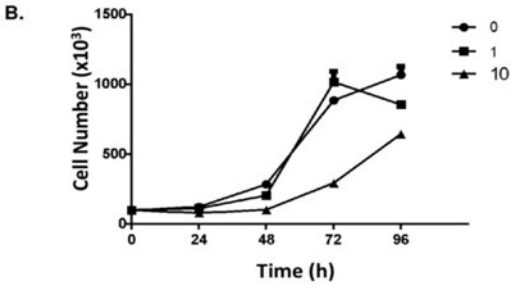

ROSC (µM) Time (h)	0	1	10
0	100	100	100
24	123	113	80
48	285	205	103
72	886	1016	295
96	1068	856	645

*The average of 3 independent experiments was taken.

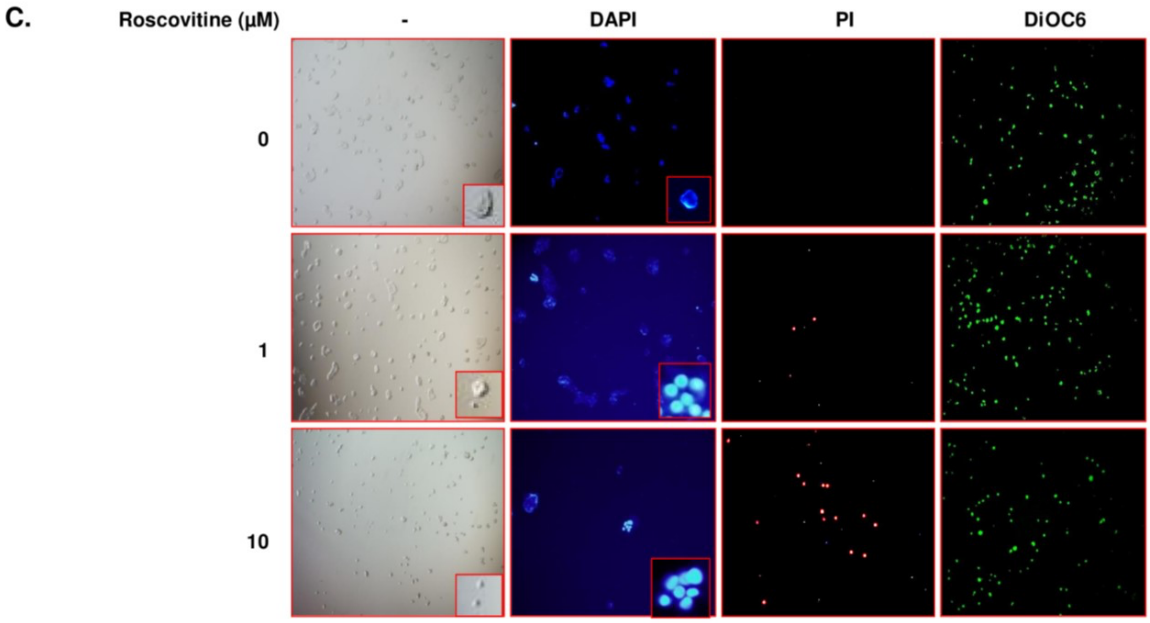

Fig. 1. The effects of ROSC administration on SK-N-AS cell viability. A. Cells were incubated with different concentrations of ROSC (0-50 µM) for 24 h and then analyzed with MTT assay. Results presented as the average of 3 independent experiments with 4 replicates. **B.** 0, 1, and 10 µM ROSC were applied to SK-N-AS cells in a time-dependent manner (0-96h) and counted with a hemocytometer. **C.** SK-N-AS cells were exposed to 1 µM and 10 µM ROSC for 24 h. Later, cells were stained with DiOC6, propidium iodide (PI), and DAPI and examined under the fluorescence microscope.

3.5. ROSC inhibited GSK-3β signaling and prevented the nuclear translocation of β-catenin

Since ROSC-induced apoptosis was clarified in the SK-N-AS cell line, western blotting analysis was performed to determine whether ROSC affected GSK-3β signaling. Total protein isolation was performed from SK-N-AS cells treated with 1 and 10 µM ROSC with the control group, and 25 µg protein sample per well was separated in 12% SDS-PAGE gels. After the immunoblotting protocols, the membranes were visualized with the help of chemiluminescence to detect the protein bands. To enlighten GSK3β signaling, we detected GSK3β, pGSK3β from the Ser9 domain, β-catenin. Histone H3 and β-actin were used as loading controls. Cells treated with 1 and 10 µM ROSC exhibited a decreased GSK3β expression dose-dependently.

On the other hand, the inhibitory phosphorylation of GSK3β from the Ser9 domain was increased dose-dependently as well compared to control samples, suggesting that GSK3β signaling was disrupted in response to ROSC treatment in SK-N-AS cells (Fig. 5A). Accordingly, the downstream target of GSK3β signaling and a vital transcription factor with the cancer progression and metastasis-inducing roles, β-catenin expression, was greatly diminished significantly after 10 μM ROSC treatment. Further, we investigated the nuclear translocation of β-catenin in response to ROSC treatment. Our results indicated that 10 μM of ROSC treatment significantly reduced the expression of β-catenin in the nucleus, suggesting ROSC prevented nuclear translocation (Fig. 5B).

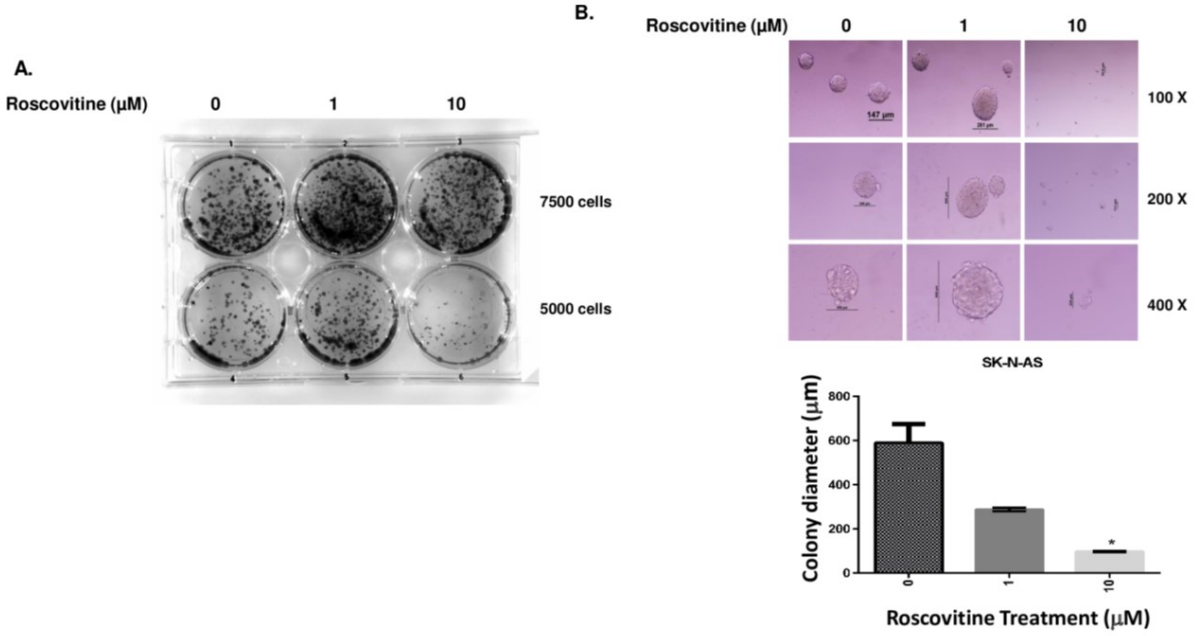

Fig. 2. The effect of ROSC treatment on colony formation potential of SK-N-AS cells. A. Cells were seeded at a concentration of either $5x10^3$ or $7.5x10^3$/ well and treated with increased concentrations of ROSC for 24h. A colony formation assay was performed, and cells were stained with crystal violet. The experiment was repeated at least three times, and the representative image was given. **B.** Neuroblastoma cells treated with 1 and 10 μM ROSC for 24 h were analyzed with soft agar colony formation assay, and the diameter of each colony was examined under a light microscope.

4. Discussion

NB, one of the most common solid tumor types of infancy, originates from the malignancy of neural crest cells that affect young children at the diagnosed age of 17 months. The heterogeneity of the tumor-initiating cells provokes therapy resistance, consequences of disseminated metastasis, and poor survival. The current treatment strategies include surgery, chemotherapy, and/ or radiation therapy for NB patients. However, almost half of the high-risk patients might face low survival lengths due to tumor recurrence due to failures of conventional therapy strategies (47). Therefore, the identification of novel treatment approaches is urgently required based on identifying key drivers for the arising of NB cells and the molecular pathways behind them. For instance, previous studies have indicated that anaplastic lymphoma kinase (ALK) is the second key driver for NB development, and its inhibition has been the furthest therapy approach in clinical applications (48).

Several studies have analyzed that GSK3β is a serine-threonine kinase that has a critical role in human cancers, either tumor promoter or suppressor manner (49). GSK3-β plays a role in the initiation and progression of NB via correlated key signaling pathways: Wnt, MAPK, PI3K/AKT/mTOR, and p53 (49–51). Also, the GSK3β expression is highly correlated with the MYCN expression, which is the crucial oncogenic driver of NB. Moreover, the intersection of GSK3-β with ALK is the second crucial oncogenic driver for NB (52). Similarly, the other tau kinases harboring the Src kinase family, mitogen-activated kinases (MAPK), and cyclin-dependent kinase 5 (CDK5) have been seen as a target for inhibition of tau phosphorylation (37,53). Given this knowledge, GSK3-β inhibition has been considered a potential therapeutic target for NB progression. Several studies indicated that inhibition of GSK3-β resulted in decreasing proliferation potential of NB cells (47,54). The anti-proliferative effect of LY2090314 has been demonstrated, one type of a GSK-3 inhibitor in NB cell lines harboring SK-N-AS, SH-SY-5Y, and NGP (47). Moreover, the dual inhibition of GSK3-β and CDK5 has also been studied for developing promising neuroprotective strategies in both *in vitro* and *in vivo* studies (55). To date, two GSK3 beta inhibitors, Tideglusib and LY2090314, have been proposed to be well-tolerated drug candidates for the clinic (56).

ROSC is one type of CDK inhibitor (CDK1,2,5,7 and 9) and blocks the cell cycle at G1/ S or G2/M stages based on time-, dose- and cell type-dependent manner (31,57,58). For instance, Kolodziejski and colleagues showed that ROSC induces cell cycle arrest at the G2/M phase in A172 and G28 glioblastoma cell lines (59). The study indicated that ROSC has therapeutic potential in various types of cancer, both preclinical and clinical stages. Several studies have also detected the synergistic effect of ROSC and other anti-cancer agents (60). For instance, Pandey and colleagues showed in their 2019 study that a combination of ROSC and temozolomide restricts the growth of glioma cells via enhancing caspase-mediated apoptosis and autophagy mechanism (61).

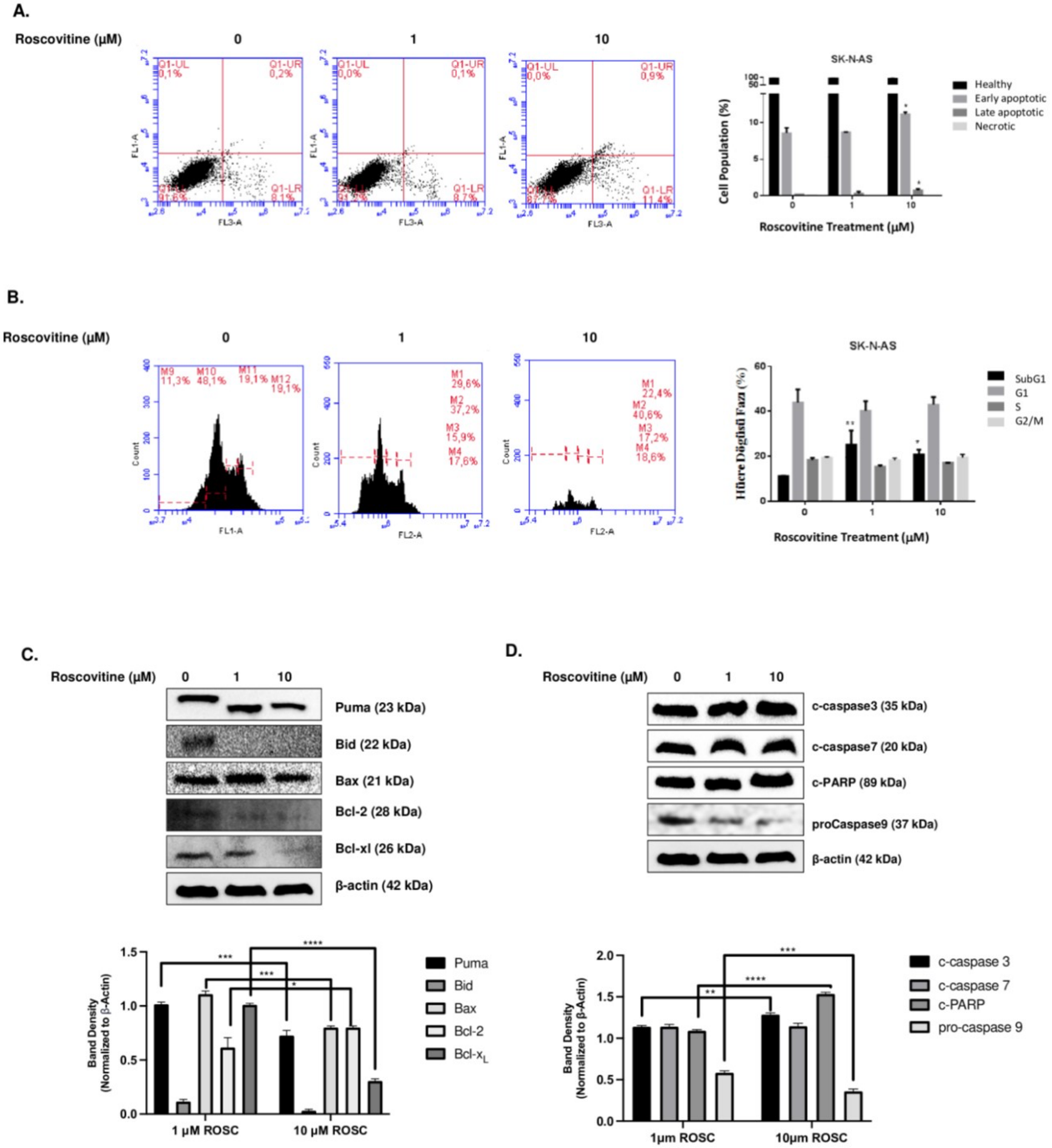

Fig. 3. ROSC induced apoptosis in a caspase9-dependent way and downregulated pro-apoptotic Bcl-2 family members in SK-N-AS cells. **A.** Annexin V-PI staining was performed to determine apoptotic cell populations. Annexin V-FITC and PI fluorescence were reported on the x-axis and y-axis, respectively. Numbers presented in the four quadrants represent the percentage of viable (lower left), necrotic (upper left), early apoptotic (lower right), and late apoptotic (upper right) cells in SK-N-AS cells. **B.** Cells were treated with 1 and 10 μM of ROSC, and the flow cytometry analysis for cell cycle phase distribution was performed following PI staining in SK-N-AS cells. **C. and D.** Increased concentrations of ROSC treatment were performed in the SK-N-AS cell line, and total protein isolation was performed. A total of 25 μg of protein was separated

with 12% SDS-PAGE. After the immunoblotting procedures, the bands of the relevant proteins were determined by the chemiluminescence method. β-actin was used as a loading control.

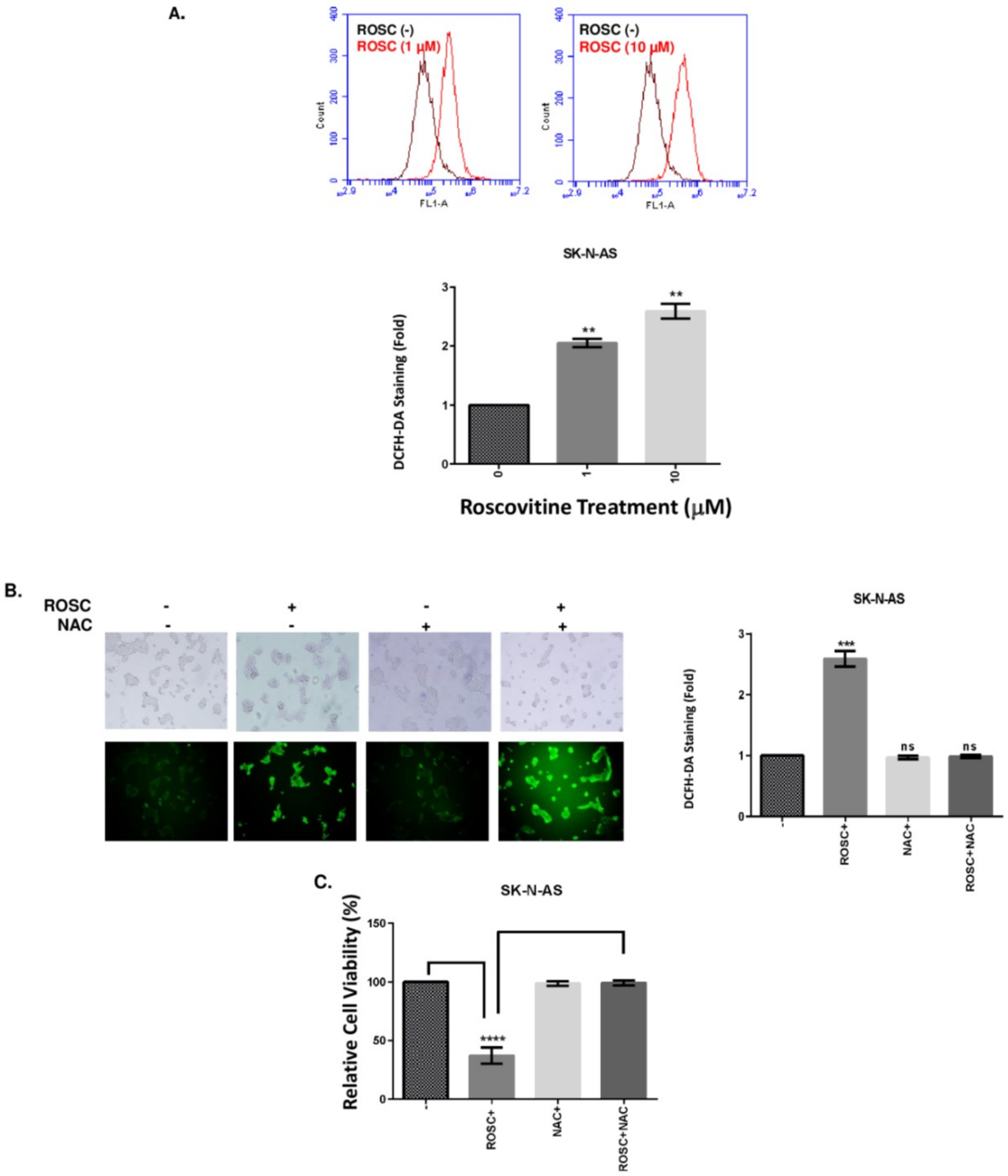

Fig. 4. Demonstration of the involvement of ROS in ROSC-induced cell death in SK-N-AS cells. A. The flow cytometric analysis of DCFH-DA staining was analyzed in the presence and absence of ROSC in the SK-N-AS cell line. **B.** NAC effect on ROS generation after dose-dependent treatment of ROSC was examined after DCFH-DA staining in SK-N-AS cells. **C.** The analysis of DCFH-DA staining after combined treatment of NAC and ROSC was evaluated with flow cytometry, and the results of three independent experiments were given as a graph.

Within the scope of this study, while investigating the role of ROSC to induce apoptosis in NB cells, this study also aimed to reveal downstream targets after ROSC administration. In this regard, firstly, we aimed to put forward the effect of ROSC to diminish the cell viability of NB cells. Our results showed that ROSC significantly inhibited the proliferation of human SK-N-AS cells in a time- and dose-dependent manner. The IC50 values of ROSC change between 15-100 µM in the literature on various types of cancer (31,57,59). For instance, 20 µM ROSC doses have been selected for HeLa and HCT116 cancer cell lines (62,63).

Moreover, Goodyear and colleagues have used 10µg/ml of ROSC for the MDA-MB-231 cell line (64). The cytostatic

effect of 25µM ROSC has been indicated in SH-SY-5Y cells, one of the NB cell lines used in the literature (65). Based on the previous data, the sub-toxic concentration range of ROSC is 5-20 µM for brain cell lines (61). In our study, we observed that 20% to 50% decreased cell viability of the SK-N-AS cells after administration of 1µM and 10µM ROSC, respectively. We further analyzed the effect on ROSC (1 µM and 10 µM) in long-term colony formation assay. Our results indicated that 10 µM ROSC significantly diminished the colony formation potential of the SK-N-AS cells as the parallel colony formation result of the U87 and C6 rat glioma cell line published by Pandey and colleagues (61). A significant decrease was detected in the colony diameters with the application of 1 and 10 µM ROSC. These results confirmed the anti-proliferative effect of ROSCs within cytotoxic doses (1 and 10 µM) in SK-N-AS cell lines for subsequent experiments.

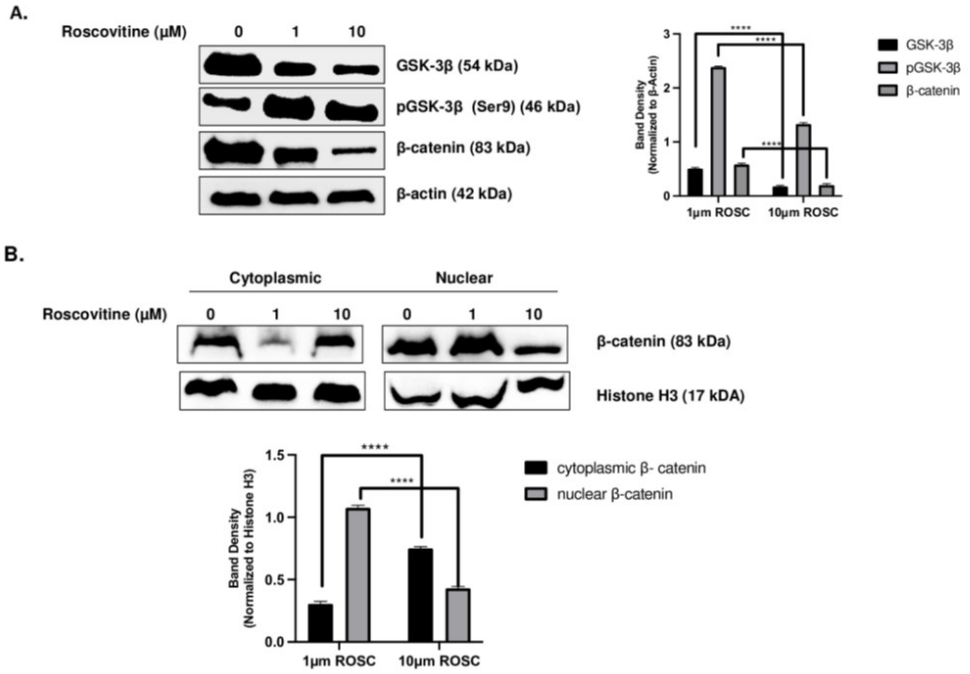

Fig. 5. Demonstration of the efficacy of ROSC administration on GSK3β signaling. Total protein isolation was performed after increasing concentrations of ROSC in SK-N-AS cells for 24 h. A 25-µg protein sample was prepared for each well and subjected to 12% SDS-PAGE separation. After the immunoblotting procedures, the bands of relevant proteins were visualized by the chemiluminescence activity of the secondary antibodies. β-actin was used as a loading control. Histone H3 was used as a nuclear fraction loading control.

Several investigations have proposed anti-proliferative and anti-apoptotic properties of ROSC as both solid and hematological malignancies (66). The study of Ozfiliz-Kilbas et al. revealed that ROSC triggers apoptosis and autophagy rely on unfolded protein response in HeLa cervical cancer cell lines (63). The other aim of our study was to enlighten the cell death mechanism type as a result of ROSC administration in NB cells. Similar to our results, a previous study showed that ROSC exhibited a dose-dependent G2/M and sub-G1 fraction increase in the A172 cell line (59). Studies investigating the effect of ROSC on cell cycle phase distribution in colorectal cancer cells have revealed that the drug can block the cell cycle in every stage by causing apoptotic induction (67).

Similarly, our flow cytometer results of annexin V-PI double staining indicated increasing sub-G1 populations after the ROSC treatment, thus inducing cell death. Apoptotic biomarkers were also analyzed to confirm whether loss of cell viability induced by ROSC resulted from apoptotic cell death. The Bcl-2 family members, either pro- or anti-apoptotic, have critical roles in intrinsic and extrinsic apoptosis pathways. Previous studies indicated that ROSC administration resulted in the expression changes of these family members (65,68). For instance, in ROSC-treated B-cell chronic lymphocytic leukemia cell lines, Mcl-1 expression, a member of the anti-apoptotic family, was downregulated, whereas Bax, a pro-apoptotic protein, was upregulated (69). The high expression of Bcl-2 proteins has been indicated in NB tissues, and it has been suggested that the decrease in Bcl-2 expression should result from a therapeutic intervention for NB (70,71). For this purpose, we investigated the expression changes of apoptotic markers by immunoblotting. 1 and 10 µM ROSC treatments significantly reduced Bcl-2 and Bcl-xL. Whereas pro-apoptotic marker expressions, Bax and Puma, were increased.

On the other hand, Bid truncation was also observed. Truncated Bid is a pro-apoptotic protein that can be induced via the activation of caspase, a member of the extrinsic

apoptotic pathway. ROSC and extrinsic apoptotic pathway correlation have been investigated in previous studies. For example, in the study of Kim et al. ROSC treatment promotes TRAIL (tumor necrosis factor-related apoptosis-inducing ligand) induced apoptosis in glioma cells, U87MG, and T98 (72). Our data showing the involvement of caspases and PARP cleavage indicated the caspase-dependent apoptosis following ROSC administration to SK-NAS cells., In the literature, ROSC-induced mitochondria-mediated and caspase-dependent apoptosis have been investigated (61,62). In the Arisan et al. study, ROSC-induced apoptotic cell death was caspase-dependent in the MCF-7 cell line (62). The increased expression of cleaved caspase families, PARP, and decreased expression of pro-caspases have been detected during the induction of apoptosis in many studies (61,62). These results demonstrated ROSC-induced mitochondria-dependent apoptosis in the SK-N-AS cell line.

Based on the existing knowledge in literature, elevated levels of ROS have been detected in cancer cells, and it is induced in various types of programmed cell death (73). In the next step of our study, we elucidated whether ROSC affected ROS generation through apoptotic induction in the SK-N-AS cell line. The relationship between ROS production and CDK5 activation, a ROSC target, has been analyzed in the HEK293 cell line in the Sandoval et al. (2018) study. Their research evaluated that the direct activation of CDK5 increased ROS production in the HEK293 cell line (74). According to our data, ROS generation increased significantly following each concentration of ROSC. Compared to ROSC alone, the combination of ROSC with NAC, a well-known ROSC scavenger, significantly prevented cell viability loss in NB cells. These results suggested that ROSC is an agent that led to the formation of ROS in SK-N-AS cell lines. Moreover, our data also put forward that NAC reversed the cytotoxic effect of ROSC by preventing intercellular ROS production when combined. According to the literature, the protective effect of NAC from oxidative stress has been elucidated in SH-SY-5Y and HepG2 cell lines (75) (76).

GSK3β is the one key signaling mediator in various cellular processes such as DNA repair, cell cycle, cell proliferation, cell signaling, and metabolic pathways. Therefore, many studies suggested that GSK3β plays a crucial role in cancer therapy. It is also involved in multiple signaling pathways, as mentioned above. According to previous findings, GSK3β has either a tumor-promoting or suppressive role, depending on the cell type (77). Kotliovara et al. indicated that the inhibition of GSK3β leads to glioma cell death via induction of apoptosis. In another study by Dickey A. et al., GSK3β inhibition promoted the induction of apoptosis in the Neuro-2A cell line (78). In our study, when cells were exposed to 10 μM ROSC, the expression of GSK3β was decreased with a subsequent increase in the expression of the phosphorylated form of GSK3β from Ser9. This result suggested that ROSC might diminish GSK3β activity. The inhibition of GSK3β has been shown to cause β-catenin, a downstream target of GSK3β, stabilization and accumulation in the cytosol. Therefore, its nuclear translocation and gene expression regulating role is prevented [(51). Aberrant nuclear accumulation of GSK3β has been previously analyzed as a hallmark of cancer in various malignant tumors (56). The reduction of β-catenin nuclear translocation via Wnt signaling inhibition has been an accepted marker of cell survival of many neuronal and cancer cell lines (75,79). Therefore, the further step of our study was to investigate the expression changes of β-catenin in both cytosolic and nuclear localization after the ROSC treatment. Also, we revealed that β-catenin levels in SK-N-AS cells were downregulated progressively in the cytoplasm and increased in the nucleus after 1 μM ROSC treatment.

On the contrary, when the cells were exposed to 10 μM ROSC, β-catenin expression was lowered from the cytoplasm to the nucleus. As a result, it is suggested that ROSC promotes apoptosis by inhibiting GSK-3β and β-catenin in SK-N-AS cell lines. The inhibitors of β-catenin signaling that can cause β-catenin downregulation, promoting ubiquitination or nuclear translocation blockage, have been accepted as anti-cancer drug candidates with therapeutic efficacy (80). ROSC, as well, has also been investigated for the effect of β-catenin expression and translocation. Studies showed that ROSC is a good candidate drug acting on β-catenin signaling in several cancer cells including prostate and cervical cancers (81,82). However, the exact relation has not been bridged in different cancer types, including NB.

Consequently, our results suggested that ROSC decreases NB cell viability and shrinks the NB cell colony diameters while inducing apoptosis. In addition, ROSC also elevated reactive oxygen generation (ROS) production, which can be prevented by N-acetyl-cysteine (NAC). ROSC also inhibited GSK3β signaling, which was proved by inhibiting the nuclear translocation of β-catenin as the downstream target transcription factor of GSK3β signaling after 10 μM ROSC treatment. These results proved that ROSC administration triggers the intrinsic apoptotic cell death by triggering ROS production, and it also affected GSK3β signaling and prevented β-catenin translocation to the nucleus in SK-N-AS cell lines. A further step of our study requires detailed data regarding the CDK5 and GSK3β-related signaling pathways of ROSC to develop a new therapeutic modality for NB.

Conflict of interest

No conflict of interest was declared by the authors.

Ethical statement

This work does not involve any animal or human subjects. The authors are aware of the details of the research that are presented in the current manuscript and gave their consent to the publication.

Funding

No funding was used for the study.

Acknowledgments
None to declare.

Authors' contributions
Concept: P.O.Y., E.D.A., Design: P.O.Y., Data Collection or Processing: Z.D., E.K., N.D., B.G., A.K.G., Analysis or Interpretation: P.O.Y., E.D.A., Literature Search: Z.D., E.K., N.D., B.G., A.K.G., P.O.Y., Writing: Z.D., E.K., N.D., A.K.G., E.D.A., P.O.Y.

References

1. Van Arendonk KJ, Chung DH. Neuroblastoma: Tumor Biology and Its Implications for Staging and Treatment. Children (Basel). 2019 Jan 17;6(1).
2. Barr EK, Applebaum MA. Genetic Predisposition to Neuroblastoma. Children (Basel). 2018 Aug 31;5(9).
3. Park JR, Eggert A, Caron H. Neuroblastoma: biology, prognosis, and treatment. Hematol Oncol Clin North Am. 2010 Feb;24(1):65–86.
4. Maris JM. Recent advances in neuroblastoma. N Engl J Med. 2010 Jun 10;362(23):2202–11.
5. Brodeur GM. Neuroblastoma: biological insights into a clinical enigma. Nat Rev Cancer. 2003 Mar;3(3):203–16.
6. Yue ZX, Huang C, Gao C, Xing TY, Liu SG, Li XJ, et al. MYCN amplification predicts poor prognosis based on interphase fluorescence in situ hybridization analysis of bone marrow cells in bone marrow metastases of neuroblastoma. Cancer Cell Int [Internet]. 2017 Mar 31 [cited 2023 Jul 24];17(1):43. Available from: /pmc/articles/PMC5374581/
7. Trigg RM, Turner SD. ALK in Neuroblastoma: Biological and Therapeutic Implications. Cancers (Basel) [Internet]. 2018 Apr 1 [cited 2023 Jul 24];10(4). Available from: /pmc/articles/PMC5923368/
8. J Ribelles A, Barberá S, Yáñez Y, Gargallo P, Segura V, Juan B, et al. Clinical Features of Neuroblastoma with 11q Deletion: An Increase in Relapse Probabilities in Localized and 4S Stages. Scientific Reports 2019 9:1 [Internet]. 2019 Sep 24 [cited 2023 Jul 24];9(1):1–9. Available from: https://www.nature.com/articles/s41598-019-50327-5
9. Attiyeh EF, London WB, Mossé YP, Wang Q, Winter C, Khazi D, et al. Chromosome 1p and 11q Deletions and Outcome in Neuroblastoma. New England Journal of Medicine. 2005 Nov 24;353(21):2243–53.
10. Duffy DJ, Krstic A, Schwarzl T, Higgins DG, Kolch W. GSK3 inhibitors regulate MYCN mRNA levels and reduce neuroblastoma cell viability through multiple mechanisms, including p53 and Wnt signaling. Mol Cancer Ther [Internet]. 2014 Feb 1 [cited 2023 Jul 24];13(2):454–67. Available from: https://dx.doi.org/10.1158/1535-7163.MCT-13-0560-T
11. Dickey A, Schleicher S, Leahy K, Hu R, Hallahan D, Thotala DK. GSK-3β inhibition promotes cell death, apoptosis, and in vivo tumor growth delay in neuroblastoma Neuro-2A cell line. J Neurooncol. 2011 Aug;104(1):145–53.
12. Kunnimalaiyaan S, Schwartz VK, Jackson IA, Clark Gamblin T, Kunnimalaiyaan M. Antiproliferative and apoptotic effect of LY2090314, a GSK-3 inhibitor, in neuroblastoma in vitro. BMC Cancer [Internet]. 2018 May 11 [cited 2023 Jul 24];18(1):1–8. Available from: https://bmccancer.biomedcentral.com/articles/10.1186/s12885-018-4474-7
13. Wu YY, Hsieh CT, Chiu YM, Chou SC, Kao JT, Shieh DC, et al. GSK-3 inhibitors enhance TRAIL-mediated apoptosis in human gastric adenocarcinoma cells. PLoS One [Internet]. 2018 Dec 1 [cited 2023 Jul 24];13(12). Available from: /pmc/articles/PMC6296518/
14. Li H, Huang K, Liu X, Liu J, Lu X, Tao K, et al. Lithium Chloride Suppresses Colorectal Cancer Cell Survival and Proliferation through ROS/GSK-3í µí»½/NF-í µí¼ B Signaling Pathway. 2014 [cited 2023 Jul 24]; Available from: http://dx.doi.org/10.1155/2014/241864
15. Wang Y, Zhang Q, Wang B, Li · Peng, Liu · Pinan. LiCl Treatment Induces Programmed Cell Death of Schwannoma Cells through AKT- and MTOR-Mediated Necroptosis. Neurochem Res. 2017;3:2363–71.
16. Wang L, Li J, Di L jun. Glycogen synthesis and beyond, a comprehensive review of GSK3 as a key regulator of metabolic pathways and a therapeutic target for treating metabolic diseases. Med Res Rev [Internet]. 2022 Mar 1 [cited 2023 Jul 24];42(2):946. Available from: /pmc/articles/PMC9298385/
17. Hur EM, Zhou FQ. GSK3 signaling in neural development. Nat Rev Neurosci [Internet]. 2010 Aug [cited 2023 Jul 24];11(8):539. Available from: /pmc/articles/PMC3533361/
18. Valenta T, Hausmann G, Basler K. The many faces and functions of β-catenin. EMBO J [Internet]. 2012 Jun 6 [cited 2023 Jul 24];31(12):2714. Available from: /pmc/articles/PMC3380220/
19. Tejeda-Muñoz N, Robles-Flores M. Glycogen synthase kinase 3 in Wnt signaling pathway and cancer. IUBMB Life [Internet]. 2015 Dec 1 [cited 2023 Jul 24];67(12):914–22. Available from: https://onlinelibrary.wiley.com/doi/full/10.1002/iub.1454
20. Fernandes JC, Rodrigues Alves APN, Machado-Neto JA, Scopim-Ribeiro R, Fenerich BA, da Silva FB, et al. IRS1/β-Catenin Axis Is Activated and Induces MYC Expression in Acute Lymphoblastic Leukemia Cells. J Cell Biochem [Internet]. 2017 Jul 1 [cited 2023 Jul 24];118(7):1774–81. Available from: https://pubmed.ncbi.nlm.nih.gov/27987331/
21. Jacobs KM, Bhave SR, Ferraro DJ, Jaboin JJ, Hallahan DE, Thotala D. GSK-3β: A Bifunctional Role in Cell Death Pathways. Int J Cell Biol [Internet]. 2012 [cited 2023 Jul 24];2012. Available from: /pmc/articles/PMC3364548/
22. Delehouzé C, Godl K, Loaëc N, Bruyère C, Desban N, Oumata N, et al. CDK/CK1 inhibitors roscovitine and CR8 downregulate amplified MYCN in neuroblastoma cells. Oncogene. 2014 Dec 11;33(50):5675–87.
23. Bettayeb K, Baunbæk D, Delehouze C, Loaëc N, Hole AJ, Baumli S, et al. CDK Inhibitors Roscovitine and CR8 Trigger Mcl-1 Down-Regulation and Apoptotic Cell Death in Neuroblastoma Cells. Genes Cancer. 2010 Apr;1(4):369–80.
24. Chen Z, Wang Z, Pang JC, Yu Y, Bieerkehazhi S, Lu J, et al. Multiple CDK inhibitor dinaciclib suppresses neuroblastoma growth via inhibiting CDK2 and CDK9 activity. Sci Rep. 2016 Jul 5;6:29090.
25. Huang Q, Zhong Y, Li J, Ye Y, Wu W, Chen L, et al. Kinase inhibitor roscovitine as a PB2 cap-binding inhibitor against influenza a virus replication. Biochem Biophys Res Commun. 2020 Jun 11;526(4):1143–9.
26. Le Roy L, Letondor A, Le Roux C, Amara A, Timsit S. Cellular and Molecular Mechanisms of R/S-Roscovitine and CDKs Related Inhibition under Both Focal and Global Cerebral Ischemia: A Focus on Neurovascular Unit and Immune Cells. Cells. 2021 Jan 8;10(1).
27. Jorda R, Paruch K, Krystof V. Cyclin-dependent kinase inhibitors inspired by roscovitine: purine bioisosteres. Curr Pharm Des. 2012;18(20):2974–80.

28. Bukanov NO, Moreno SE, Natoli TA, Rogers KA, Smith LA, Ledbetter SR, et al. CDK inhibitors R-roscovitine and S-CR8 effectively block renal and hepatic cystogenesis in an orthologous model of ADPKD. Cell Cycle. 2012 Nov 1;11(21):4040–6.

29. Meijer L, Raymond E. Roscovitine and other purines as kinase inhibitors. From starfish oocytes to clinical trials. Acc Chem Res. 2003 Jun;36(6):417–25.

30. Le Moigne V, Rodriguez Rincon D, Glatigny S, Dupont CM, Langevin C, Ait Ali Said A, et al. Roscovitine Worsens Mycobacterium abscessus Infection by Reducing DUOX2-mediated Neutrophil Response. Am J Respir Cell Mol Biol. 2022 Apr;66(4):439–51.

31. Cicenas J, Kalyan K, Sorokinas A, Stankunas E, Levy J, Meskinyte I, et al. Roscovitine in cancer and other diseases. Ann Transl Med. 2015 Jun;3(10):135.

32. Araki T, Liu NA. Cell Cycle Regulators and Lineage-Specific Therapeutic Targets for Cushing Disease. Front Endocrinol (Lausanne). 2018;9:444.

33. Tirado OM, Mateo-Lozano S, Notario V. Roscovitine is an effective inducer of apoptosis of Ewing's sarcoma family tumor cells in vitro and in vivo. Cancer Res. 2005 Oct 15;65(20):9320–7.

34. Ryder J, Su Y, Liu F, Li B, Zhou Y, Ni B. Divergent roles of GSK3 and CDK5 in APP processing. Biochem Biophys Res Commun. 2003 Dec 26;312(4):922–9.

35. Liu J, Yang J, Xu Y, Guo G, Cai L, Wu H, et al. Roscovitine, a CDK5 Inhibitor, Alleviates Sevoflurane-Induced Cognitive Dysfunction via Regulation Tau/GSK3β and ERK/PPARγ/CREB Signaling. Cell Physiol Biochem. 2017;44(2):423–35.

36. Maldonado H, Ramírez E, Utreras E, Pando ME, Kettlun AM, Chiong M, et al. Inhibition of cyclin-dependent kinase 5 but not of glycogen synthase kinase 3-β prevents neurite retraction and tau hyperphosphorylation caused by secretable products of human T-cell leukemia virus type I-infected lymphocytes. J Neurosci Res. 2011 Sep;89(9):1489–98.

37. Obakan Yerlikaya P, Arısan ED, Coker Gurkan A, Okumus OO, Yenigun T, Ozbey U, et al. Epibrassinolide prevents tau hyperphosphorylation via GSK3β inhibition in vitro and improves Caenorhabditis elegans lifespan and motor deficits in combination with roscovitine. Amino Acids. 2021 Sep 1;53(9):1373–89.

38. Adacan K, Obakan-Yerlikaya P, Arisan ED, Coker-Gurkan A, Kaya RI, Palavan-Unsal N. Epibrassinolide-induced autophagy occurs in an Atg5-independent manner due to endoplasmic stress induction in MEF cells. Amino Acids [Internet]. 2020 Jul 1 [cited 2022 May 12];52(6–7):871–91. Available from: https://pubmed.ncbi.nlm.nih.gov/32449072/

39. Obakan-Yerlikaya P, Arisan ED, Coker-Gurkan A, Adacan K, Ozbey U, Somuncu B, et al. Calreticulin is a fine tuning molecule in epibrassinolide-induced apoptosis through activating endoplasmic reticulum stress in colon cancer cells. Mol Carcinog [Internet]. 2017 Jun 1 [cited 2022 May 12];56(6):1603–19. Available from: https://pubmed.ncbi.nlm.nih.gov/28112451/

40. Capik O, Gundogdu B, Tatar A, Sahin A, Chen F, Creighton CJ, et al. Oncogenic miR-1825 promotes head and neck carcinogenesis via targeting FREM1. J Cell Biochem [Internet]. 2023 [cited 2023 Sep 19]; Available from: https://pubmed.ncbi.nlm.nih.gov/37683055/

41. Li Q, Zhu Z, Zhang H, Wu X, Yang H, Li X, et al. LncRNA RP11-93B14.5 promotes gastric cancer cell growth through PI3K/AKT signaling pathway. Mol Biotechnol [Internet]. 2023 [cited 2023 Sep 19]; Available from: https://pubmed.ncbi.nlm.nih.gov/37682457/

42. Coker-Gürkan A, Arisan ED, Obakan P, Akalin K, Özbey U, Palavan-Unsal N. Purvalanol induces endoplasmic reticulum stress-mediated apoptosis and autophagy in a time-dependent manner in HCT116 colon cancer cells. Oncol Rep. 2015 Jun 1;33(6):2761–70.

43. Weidner C, Rousseau M, Plauth A, Wowro SJ, Fischer C, Abdel-Aziz H, et al. Iberis amara Extract Induces Intracellular Formation of Reactive Oxygen Species and Inhibits Colon Cancer. PLoS One [Internet]. 2016 Apr 1 [cited 2023 Sep 19];11(4):e0152398. Available from: https://journals.plos.org/plosone/article?id=10.1371/journal.pone.0152398

44. Lin S, Lv J, Peng P, Cai C, Deng J, Deng H, et al. Bufadienolides induce p53-mediated apoptosis in esophageal squamous cell carcinoma cells in vitro and in vivo. Oncol Lett. 2018 Feb 1;15(2):1566–72.

45. Chen D, Chen C, Huang C, Chen T, Liu Z. Injectable Hydrogel for NIR-II Photo-Thermal Tumor Therapy and Dihydroartemisinin-Mediated Chemodynamic Therapy. Front Chem. 2020 Apr 7;8.

46. Obakan P, Arisan ED, Calcabrini A, Agostinelli E, Bolkent Ş, Palavan-Unsal N. Activation of polyamine catabolic enzymes involved in diverse responses against epibrassinolide-induced apoptosis in LNCaP and DU145 prostate cancer cell lines. Amino Acids [Internet]. 2014 [cited 2022 May 12];46(3):553–64. Available from: https://pubmed.ncbi.nlm.nih.gov/23963538/

47. Kunnimalaiyaan S, Schwartz VK, Jackson IA, Clark Gamblin T, Kunnimalaiyaan M. Antiproliferative and apoptotic effect of LY2090314, a GSK-3 inhibitor, in neuroblastoma in vitro. BMC Cancer. 2018 May 11;18(1).

48. Otte J, Dyberg C, Pepich A, Johnsen JI. MYCN Function in Neuroblastoma Development. Vol. 10, Frontiers in Oncology. Frontiers Media S.A.; 2021.

49. Sahin I, Eturi A, De Souza A, Pamarthy S, Tavora F, Giles FJ, et al. Glycogen synthase kinase-3 beta inhibitors as novel cancer treatments and modulators of antitumor immune responses. Vol. 20, Cancer Biology and Therapy. Taylor and Francis Inc.; 2019. p. 1047–56.

50. Bahmad HF, Chalhoub RM, Harati H, Bou-Gharios J, Assi S, Ballout F, et al. Tideglusib attenuates growth of neuroblastoma cancer stem/progenitor cells in vitro and in vivo by specifically targeting GSK-3β. Pharmacological Reports. 2021 Feb 1;73(1):211–26.

51. Lin J, Song T, Li C, Mao W. GSK-3β in DNA repair, apoptosis, and resistance of chemotherapy, radiotherapy of cancer. Vol. 1867, Biochimica et Biophysica Acta - Molecular Cell Research. Elsevier B.V.; 2020.

52. Gonzalez Malagon SG, Liu KJ. ALK and GSK3: Shared Features of Neuroblastoma and Neural Crest Cells. Vol. 12, Journal of Experimental Neuroscience. SAGE Publications Ltd; 2018.

53. Yadikar H, Torres I, Aiello G, Kurup M, Yang Z, Lin F, et al. Screening of tau protein kinase inhibitors in a tauopathy-relevant cell-based model of tau hyperphosphorylation and oligomerization. PLoS One. 2020 Jul 1;15(7 July).

54. Le Grand M, Kimpton K, Gana CC, Valli E, Fletcher JI, Kavallaris M. Targeting Functional Activity of AKT Has Efficacy against Aggressive Neuroblastoma. ACS Pharmacol Transl Sci. 2020 Feb 14;3(1):148–60.

55. Reinhardt L, Kordes S, Reinhardt P, Glatza M, Baumann M, Drexler HCA, et al. Dual Inhibition of GSK3β and CDK5 Protects the Cytoskeleton of Neurons from Neuroinflammatory-Mediated Degeneration In Vitro and In Vivo. Stem Cell Reports. 2019 Mar

5;12(3):502–17.

56. Walz A, Ugolkov A, Chandra S, Kozikowski A, Carneiro BA, O'Halloran T V., et al. Molecular pathways: Revisiting glycogen synthase kinase-3β as a target for the treatment of cancer. Clinical Cancer Research. 2017 Apr 15;23(8):1891–7.

57. Teusel F, Henschke L, Mayer TU. Small molecule tools in mitosis research. In: Methods in Cell Biology. Academic Press Inc.; 2018. p. 137–55.

58. Meijer L, Borgne A, Mulner O, Chong JPJ, Blow JJ, Inagaki N, et al. Biochemical and cellular effects of roscovitine, a potent and selective inhibitor of the cyclin-dependent kinases cdc2, cdk2 and cdk5. Eur J Biochem. 1997;243(1–2):527–36.

59. Kolodziej M, Goetz C, Di Fazio P, Montalbano R, Ocker M, Strik H, et al. Roscovitine has anti-proliferative and pro-apoptotic effects on glioblastoma cell lines: A pilot study. Oncol Rep. 2015 Sep 1;34(3):1549–56.

60. Mughal MJ, Bhadresha K, Kwok HF. CDK inhibitors from past to present: A new wave of cancer therapy. Vol. 88, Seminars in Cancer Biology. Academic Press; 2023. p. 106–22.

61. Pandey V, Ranjan N, Narne P, Babu PP. Roscovitine effectively enhances antitumor activity of temozolomide in vitro and in vivo mediated by increased autophagy and Caspase-3 dependent apoptosis. Sci Rep. 2019 Dec 1;9(1).

62. Arisan ED, Obakan P, Coker A, Palavan-Unsal N. Inhibition of ornithine decarboxylase alters the roscovitine-induced mitochondrial-mediated apoptosis in MCF-7 breast cancer cells. Mol Med Rep. 2012 May;5(5):1323–9.

63. Ozfiliz-Kilbas P, Sarikaya B, Obakan-Yerlikaya P, Coker-Gurkan A, Arisan ED, Temizci B, et al. Cyclin-dependent kinase inhibitors, roscovitine and purvalanol, induce apoptosis and autophagy related to unfolded protein response in HeLa cervical cancer cells. Mol Biol Rep. 2018 Oct 1;45(5):815–28.

64. Goodyear S, Sharma MC. Roscovitine regulates invasive breast cancer cell (MDA-MB231) proliferation and survival through cell cycle regulatory protein cdk5. Exp Mol Pathol. 2007 Feb;82(1):25–32.

65. Roufayel R, Murshid N. CDK5: Key regulator of apoptosis and cell survival. Vol. 7, Biomedicines. MDPI AG; 2019.

66. Pizarro JG, Folch J, Junyent F, Verdaguer E, Auladell C, Beas-Zarate C, et al. Antiapoptotic effects of roscovitine on camptothecin-induced DNA damage in neuroblastoma cells. Apoptosis. 2011;16(5):536–50.

67. McClue SJ, Blake D, Clarke R, Cowan A, Cummings L, Fischer PM, et al. In vitro and in vivo antitumor properties of the cyclin dependent kinase inhibitor CYC202 (R-roscovitine). Int J Cancer. 2002 Dec 10;102(5):463–8.

68. Garrofé-Ochoa X, Cosialls AM, Ribas J, Gil J, Boix J. Transcriptional modulation of apoptosis regulators by roscovitine and related compounds. Apoptosis. 2011 Jul;16(7):660–70.

69. Hahntow IN, Schneller F, Oelsner M, Weick K, Ringshausen I, Fend F, et al. Cyclin-dependent kinase inhibitor Roscovitine induces apoptosis in chronic lymphocytic leukemia cells. Leukemia. 2004;18(4):747–55.

70. Bierbrauer A, Jacob M, Vogler M, Fulda S. A direct comparison of selective BH3-mimetics reveals BCL-XL, BCL-2 and MCL-1 as promising therapeutic targets in neuroblastoma. Br J Cancer. 2020 May 12;122(10):1544–51.

71. Klenke S, Akdeli N, Stelmach P, Heukamp L, Schulte JH, Bachmann HS. The small molecule Bcl-2/Mcl-1 inhibitor TW-37 shows single-agent cytotoxicity in neuroblastoma cell lines. BMC Cancer. 2019 Mar 18;19(1).

72. Kim EH, Kim SU, Shin DY, Choi KS. Roscovitine sensitizes glioma cells to TRAIL-mediated apoptosis by downregulation of survivin and XIAP. Oncogene. 2004 Jan 15;23(2):446–56.

73. Perillo B, Di Donato M, Pezone A, Di Zazzo E, Giovannelli P, Galasso G, et al. ROS in cancer therapy: the bright side of the moon. Vol. 52, Experimental and Molecular Medicine. Springer Nature; 2020. p. 192–203.

74. Sandoval R, Lazcano P, Ferrari F, Pinto-Pardo N, González-Billault C, Utreras E. TNF-α increases production of reactive oxygen species through Cdk5 activation in nociceptive neurons. Front Physiol. 2018 Feb 6;9(FEB).

75. Yerlikaya PO, Naxmedova S. Epibrassinolide Triggers Apoptotic Cell Death in SK-N-AS Neuroblastoma Cells by Targeting GSK3β in a ROS Generation-Dependent Way. European Journal of Biology. 2022;81(2):240–50.

76. Yedjou CG, Tchounwou PB. N-Acetyl-L-Cysteine Affords Protection against Lead-Induced Cytotoxicity and Oxidative Stress in Human Liver Carcinoma (HepG 2) Cells [Internet]. Vol. 4, Int. J. Environ. Res. Public Health. 2007. Available from: www.ijerph.org

77. Kazi A, Xiang S, Yang H, Delitto D, Trevino J, Jiang RHY, et al. GSK3 suppression upregulates β-catenin and c-Myc to abrogate KRas-dependent tumors. Nat Commun. 2018 Dec 1;9(1).

78. Dickey A, Schleicher S, Leahy K, Hu R, Hallahan D, Thotala DK. GSK-3β inhibition promotes cell death, apoptosis, and in vivo tumor growth delay in neuroblastoma Neuro-2A cell line. J Neurooncol. 2011 Aug;104(1):145–53.

79. Tompa M, Kalovits F, Nagy A, Kalman B. Contribution of the Wnt Pathway to Defining Biology of Glioblastoma. Vol. 20, NeuroMolecular Medicine. Humana Press Inc.; 2018. p. 437–51.

80. Yu WK, Xu ZY, Yuan L, Mo S, Xu B, Cheng XD, et al. Targeting β-Catenin Signaling by Natural Products for Cancer Prevention and Therapy. Front Pharmacol [Internet]. 2020 Jun 30 [cited 2023 Jul 24];11. Available from: /pmc/articles/PMC7338604/

81. Park CS, Kim S Il, Lee MS, Youn CY, Kim DJ, Jho EH, et al. Modulation of β-Catenin Phosphorylation/Degradation by Cyclin-dependent Kinase 2. Journal of Biological Chemistry. 2004 May 7;279(19):19592–9.

82. Huang CY, Velmurugan BK, Chen MC, Day CH, Chien WS, Padma V V., et al. KHC-4 inhibits β-catenin expression in prostate cancer cells. Biotech Histochem [Internet]. 2019 Jul 4 [cited 2023 Jul 24];94(5):374–80. Available from: https://pubmed.ncbi.nlm.nih.gov/30819007/